EUROPEAN ORGANIZATION FOR NUCLEAR RESEARCH (CERN)

CERN-EP-2021-100
2022/04/28

CMS-HIN-18-008

Two-particle azimuthal correlations in γp interactions using pPb collisions at $\sqrt{s_{\mathrm{NN}}} = 8.16\,\mathrm{TeV}$

The CMS Collaboration

Abstract

The first measurements of the Fourier coefficients ($V_{n\Delta}$) of the azimuthal distributions of charged hadrons emitted from photon-proton (γp) interactions are presented. The data are extracted from $68.8\,\mathrm{nb}^{-1}$ of ultra-peripheral proton-lead (pPb) collisions at $\sqrt{s_{\mathrm{NN}}} = 8.16\,\mathrm{TeV}$ using the CMS detector. The high energy lead ions produce a flux of photons that can interact with the oncoming proton. This γp system provides a set of unique initial conditions with multiplicity lower than in photon-lead collisions but comparable to recent electron-positron and electron-proton data. The $V_{n\Delta}$ coefficients are presented in ranges of event multiplicity and transverse momentum (p_{T}) and are compared to corresponding hadronic minimum bias pPb results. For a given multiplicity range, the mean p_{T} of charged particles is smaller in γp than in pPb collisions. For both the γp and pPb samples, $V_{1\Delta}$ is negative, $V_{2\Delta}$ is positive, and $V_{3\Delta}$ consistent with 0. For each multiplicity and p_{T} range, $V_{2\Delta}$ is larger for γp events. The γp data are consistent with model predictions that have no collective effects thus suggesting the absence of collectivity in the γp system over the multiplicity range explored in this work.

Submitted to Physics Letters B

1 Introduction

A wide variety of measurements suggest the existence of collectivity in the collisions of small systems such as the proton-proton (pp) [1–5] and proton-nucleus (pA) [6–17] collisions. Such collectivity could indicate the formation of a hot, strongly interacting "quark gluon plasma" (QGP), characterized by nearly ideal hydrodynamic behavior [18–20], or could alternatively arise from gluon saturation in the initial state [21, 22]. Properties of the QGP have been previously studied in a wide range of high-energy nucleus-nucleus (AA) collisions at the CERN LHC and BNL RHIC [23–31]. In these studies, collectivity is observed via the azimuthal correlations of particles that are far apart in rapidity. This phenomenon is known as the "ridge" [21], and has been observed in pp and pPb collisions that produce at least 110 charged particles in the final state [1–17]. The two-particle azimuthal correlations can be characterized by their Fourier components ($V_{n\Delta}$) where n represents the order of the moment. If the two-particle correlations can be factorized into the product of the corresponding single particle azimuthal distributions, then the single-particle azimuthal anisotropy Fourier coefficients v_n can be extracted as $v_n = \sqrt{V_{n\Delta}}$ [32]. The second (v_2) and third (v_3) coefficients are known as elliptic and triangular flow, respectively, and are directly related to the initial collision geometry and its fluctuations, which influence the medium evolution and and provide information about its fundamental transport properties [33–36].

In high-multiplicity events, v_2 and v_3 depend upon the hadron species [15, 37–41] and scale with the number of valence quarks in the hadron [15]. Such results suggest a common origin of the collectivity seen in PbPb, as well as in high-multiplicity pp and pPb events, where a hydrodynamic description can be used to reasonably reproduce the measurements in each case [42–45]. Probing systems with even smaller interaction regions is therefore important to understand the reach of such a hydrodynamic description. The search for collectivity has been recently extended to electron-positron, electron-proton, and photon-nucleus interactions [46–48]. None of these systems exhibit evidence of the long-range correlations seen in hadronic collisions.

High-energy pPb ultra-peripheral collisions at the LHC, where the impact parameter is larger than the nucleus radius provide a new system to extend the search of long-range correlations to photon-proton (γp) collisions. At TeV energies, the lead (Pb) nuclei generate a very large quasi-real photon flux [49]. In the equivalent photon approximation [50–52], this flux can be considered as γ beams of virtuality $Q^2 < 1/R^2$, where R is the effective radius of the charge distribution. For Pb nuclei at 2.56 TeV with radius $R \approx 7$ fm, the quasi-real photon beams have virtualities $Q^2 < 10^{-3}\,\text{GeV}^2$, but very large longitudinal energy, up to $E_\gamma = \hbar c/\alpha R \approx 80\,\text{GeV}$, where α is the reciprocal Lorentz relativistic factor.

This Letter presents a first search for long-range correlations and the first measurement of $V_{n\Delta}$ coefficients for the γp system. The CMS detector has been used to collect a large sample of γp interactions that occur in ultra-peripheral pPb collisions. The beam energies were 6.50 TeV for the protons and 2.56 TeV per nucleon for the Pb nuclei, resulting in a center-of-mass energy per nucleon pair ($\sqrt{s_{\text{NN}}}$) of 8.16 TeV. The γp results are compared to both hadronic minimum bias (MB) pPb collisions (previously studied in Ref. [53]) and predictions of the PYTHIA v8.2 [54] model interfaced with the Delphes v3.4.2 fast simulation package [55]. The minimum bias data are compared to predictions from the HIJING v2.1 generator [56] coupled to a full GEANT4 simulation of the detector [57].

2 Experimental apparatus and data sample

The central feature of the CMS apparatus is a superconducting solenoid of 6 m internal diameter, providing a magnetic field of 3.8 T. Within the solenoid volume is the silicon tracker, a lead tungstate crystal electromagnetic calorimeter, and a brass and scintillator hadron calorimeter, each composed of a barrel and two endcap sections that cover the range $|\eta| < 3.0$. The silicon tracker measures charged particles within the range $|\eta| < 2.5$. It consists of 1440 silicon pixel and 15 148 silicon strip detector modules, and provides an impact parameter resolution of about 15 μm and a transverse momentum (p_{T}) resolution better than 1.5% at $p_{\mathrm{T}} \approx 100\,\mathrm{GeV}/c$. Event selection for this analysis makes use of detectors in the forward region: hadron forward (HF) calorimeters that use quartz fibers embedded in a steel absorber covering the region $3.0 < |\eta| < 5.2$ and the two Zero Degree Calorimeters (ZDCs) which measure neutral particles with $|\eta| > 8.3$ [58]. Analysis in the midrapidity region is based upon objects produced by the CMS particle-flow (PF) algorithm [59], which reconstructs and identifies final-state particles with an optimized combination of information from the various elements of the CMS detector. A more detailed description of the CMS detector, together with a definition of the coordinate system used and the relevant kinematic variables, can be found in Ref. [60].

The analysis is performed using data recorded by CMS during the LHC pPb run in 2016 with an integrated luminosity of 68.8 nb^{-1}. The proton-going direction is towards the side of the detector with positive η. As a result of the energy difference between the colliding beams, the nucleon-nucleon (NN) center-of-mass for pPb collisions is not at rest with respect to the laboratory frame. Massless particles emitted at $\eta_{\mathrm{cm}} = 0$ in the NN center-of-mass frame will be detected at $\eta = +0.465$ in the laboratory frame. The event samples were collected by the CMS experiment with a two-level trigger system [53] consisting in the level-1 (L1), where events are selected by custom hardware processors and the high-level trigger (HLT), that uses fast versions of the offline software.

3 Event selection

Samples of both γp-enhanced and MB events were collected requiring energy deposits in at least one of the HF calorimeters above a threshold of approximately 1 GeV at L1. The HLT system requires the presence of at least one charged particle (track) with $p_{\mathrm{T}} > 0.4\,\mathrm{GeV}/c$ in the pixel tracker. Track reconstruction was performed online as part of the HLT trigger with a reconstruction algorithm that is identical to the one used offline [61]. More details of the MB trigger can be found in Ref. [62]. For each event, the reconstructed vertex with the highest number of associated tracks was selected as the primary vertex. A zero bias trigger requiring only the presence of proton and lead bunches in the CMS detector was used to independently study the trigger efficiency ($\varepsilon_{\mathrm{trig}}$). The beam bunches were detected by induction counters placed 175 m from the interaction point on each side of the experiment. In addition, a sample of events with neither beam present was collected for noise studies.

For both γp and MB samples, the reconstructed primary vertex was required to be within 15 cm of the nominal interaction point along the beam axis (z) and within 0.15 cm in the transverse plane. Only high-purity tracks, described in Ref. [61], were used in this analysis. The impact parameter significance of reconstructed tracks with respect to the primary vertex in the longitudinal and transverse directions was required to be <3 standard deviations. Finally, the relative uncertainty in the p_{T} of the track was required to be <10%. At least two reconstructed tracks with $|\eta| < 2.4$ and $p_{\mathrm{T}} > 0.4\,\mathrm{GeV}/c$ were required to be associated with the primary vertex. Beam-related background was suppressed by rejecting events for which <25% of all

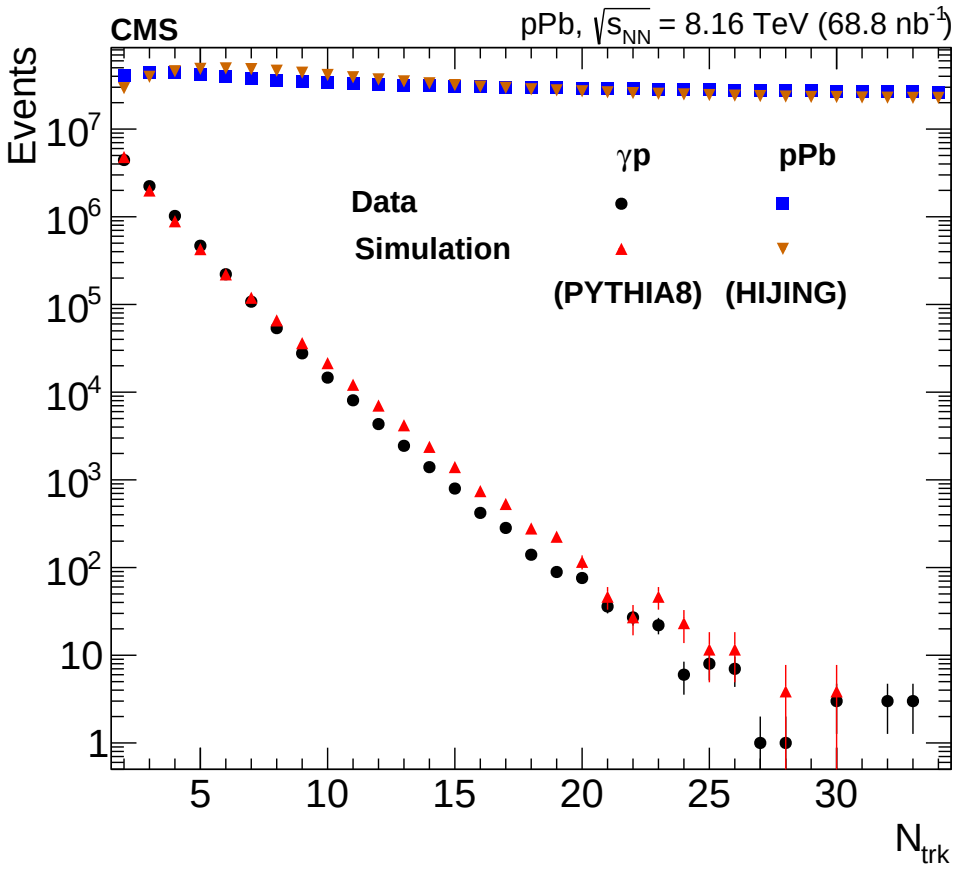

Figure 1: The N_{trk} spectra for γp and MB samples. The simulated γp distribution has been normalized to the same event yield of the data γp enhanced sample.

reconstructed tracks pass the standard track selection criteria.

Typical pPb collisions produce particles at both positive and negative rapidity [38, 53, 63]. However, γp events are expected to be very asymmetric in the laboratory frame since the photon energy is generally much smaller than the proton beam energy.

For the γp-enhanced selection, a rapidity gap is defined as a continuous region in which there is low detector activity, as done in Ref. [64]. The detector acceptance $|\eta| < 5.0$ is divided into 20 bins. Threshold values are assigned to each η bin, they delimit the energy from all PF candidates that can be considered significant and which contain at least 99.7% of detector activity caused by detector noise or by beam-gas events. These thresholds were obtained by studying the zero-bias events triggered on non-colliding bunches. For each event, a given η bin was considered to be empty if the energy registered from the PF candidates was below its assigned threshold value. For the 10 bins in the regions $|\eta| < 2.5$ the energy threshold was 6 GeV and no high-purity tracks with $p_{\text{T}} > 200$ MeV/c were allowed. Activity in the forward lead-going region $-5.0 < \eta < -3.0$ was suppressed by implementing a set of threshold values that range from 13.4 to 16.9 GeV. For the bin $-2.5 > \eta > -3.0$ only neutral hadrons were considered and the energy threshold was 13.4 GeV. The forward rapidity gap ($\Delta\eta^F$) variable was then defined as the difference from $\eta = -5.0$ to the lower edge of the first non-empty η bin.

The MB selection requires the coincidence of at least one tower with energy above 3.0 GeV

Table 1: Mean N_{trk} for the γp-enhanced and the MB data sets for five classes of N_{trk}. Statistical uncertainties are negligible.

Sample	$2 \leq N_{trk} < 5$	$5 \leq N_{trk} < 10$	$10 \leq N_{trk} < 35$	$5 \leq N_{trk} < 35$	$2 \leq N_{trk} < 35$
γp-enhanced	2.6	5.8	11.3	6.0	2.9
γp-simulated	2.6	5.9	11.4	6.2	2.9
MB	3.0	6.9	21.5	18.5	16.6
MB-simulated	3.1	6.9	20.7	17.2	15.7

in both HF calorimeters and at least two tracks with $|\eta| < 2.5$. In contrast, a γp-enhanced selection is designed to capture events with an intact Pb nucleus, particle production in the positive η region, and a large rapidity gap [65–67]. The first two requirements are met by requiring no neutrons in the ZDC on the Pb-going side and at least 10 GeV in the highest energy tower of the HF calorimeter on the p-going side. To ensure a large rapidity gap, we require $5.0 < \Delta\eta^F < 7.5$. This corresponds to not having a particle within the negative-η region. A total of 8.6×10^6 γp-enhanced and 1.0×10^9 MB candidate events were selected. From Ref. [64] the purity of the γp-enhanced sample without the ZDC cut is estimated to be about 95%. The requirement of no neutron emission used in this analysis gives an additional suppression of pomeron-Pb events.

The reconstructed track multiplicity (N_{trk}) is defined as the number of tracks from the primary vertex with $p_T > 0.4$ GeV/c, and $|\eta| < 2.4$. Figure 1 shows the N_{trk} spectra for the γp-enhanced and MB data samples along with simulations from the PYTHIA8 and HIJING event generators. For the γp-simulated sample, the events are restricted to those with no tracks in the $\eta < 0$ region and normalized to the γp-enhanced yield. In contrast to the MB sample, the γp-enhanced spectrum drops very rapidly with multiplicity up to a limiting value of 34. The $\langle N_{trk} \rangle$ value corresponding to the $2 \leq N_{trk} < 35$ range for the γp-enhanced sample is $\approx$2.9 and about 16.6 for the MB sample. The N_{trk} distribution from the zero bias data control sample has $\langle N_{trk} \rangle \approx 0.84$. The γp-simulated sample shows a shape and range that is consistent with the γp-enhanced data sample. Three N_{trk} bins are used to analyze the γp-enhanced events: $2 \leq N_{trk} < 5$, $5 \leq N_{trk} < 10$, $10 \leq N_{trk} < 35$. The first two deliver a comparable number of particle pairs and the third one aims to probe the higher N_{trk} domain by averaging the last part of the distribution. Table 1 indicates the $\langle N_{trk} \rangle$ values for the data and simulated γp and MB samples. The mean p_T, $\langle p_T \rangle$, values of charged particles in the γp and MB data samples are 0.67 ± 0.01 and 0.74 ± 0.01 GeV/c respectively.

4 Analysis technique

To ensure a high tracking efficiency, only tracks with $0.3 < p_T < 3.0$ GeV/c are used in the analysis. The analysis techniques for two-particle correlations are identical to those used for recent measurements [3, 6, 26] and are described hereafter. For each multiplicity class, tracks tagged as "trigger particles" are those whose p_T, labeled as p_T^{trig}, is within a given range. The number of trigger particles in the event is denoted by N_{trig}. Particle pairs are then formed by associating each trigger particle with the remaining tracks within a specified $p_T = p_T^{assoc}$ interval. For this analysis, identical ranges are used for p_T^{trig} and p_T^{assoc}. Two different p_T ranges are studied, i.e. $[0.3, 3.0]$ and $[1.0, 3.0]$ GeV/c. These are the same as those used in previous studies of the ridge [6] and observations of correlations between v_n coefficients [53] in pPb collisions.

The two-dimensional correlation function is defined as

$$\frac{1}{N_{\mathrm{trig}}}\frac{\mathrm{d}^2N^{\mathrm{pair}}}{\mathrm{d}\Delta\eta\,\mathrm{d}\Delta\phi} = B(0,0)\frac{S(\Delta\eta,\Delta\phi)}{B(\Delta\eta,\Delta\phi)}, \tag{1}$$

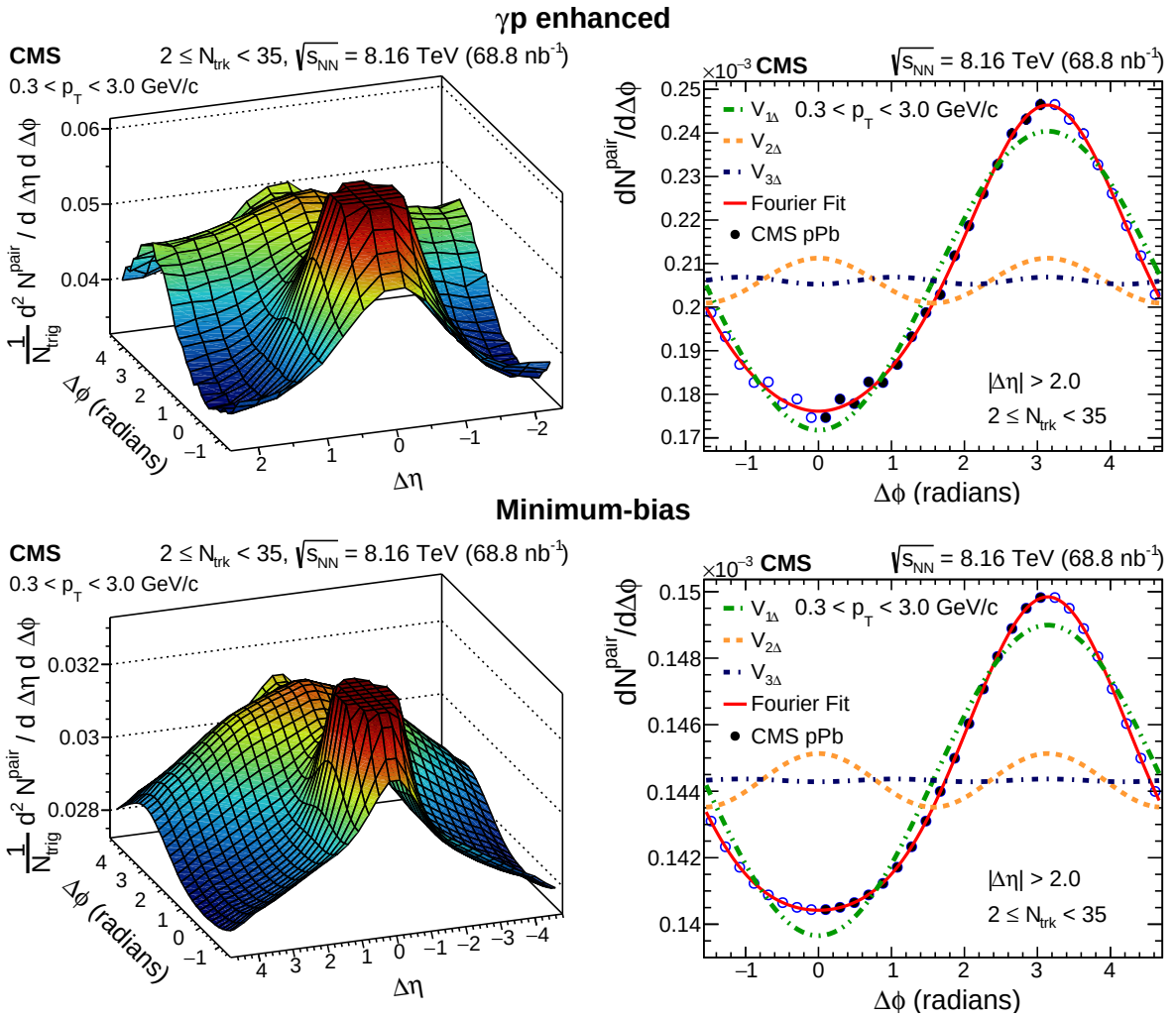

Figure 2: Two-dimensional (left) and one-dimensional (right) correlation plots for γp-enhanced (upper) and MB (lower) events for $0.3 < p_{\mathrm{T}} < 3.0\,\mathrm{GeV}/c$ and $2 \leq N_{\mathrm{trk}} < 35$. For the two-dimensional distributions, the jet peak centered at $\Delta\eta = \Delta\phi = 0$ is truncated to increase visibility. The rapidity gap requirement for the γp-enhanced sample limits the $|\Delta\eta|$ range to $|\Delta\eta| < 2.5$. The one-dimensional $\Delta\phi$ distributions are symmetrized by construction around $\Delta\phi = 0$ and π. The Fourier coefficients, $V_{n\Delta}$ in the right column are fit over the $\Delta\phi$ range $[0, \pi]$. Points outside this range are shown as open circles and are obtained by symmetrization of those in $[0, \pi]$. Statistical error bars are shown for both one-dimensional distributions.

where $\Delta\eta$ and $\Delta\phi$ are the differences in η and ϕ of the pair and N^{pair} is the number of pairs. The same-event pair distribution, $S(\Delta\eta, \Delta\phi)$, represents the yield of particle pairs from the same event in a given $(\Delta\eta, \Delta\phi)$ bin. The mixed-event pair distribution $B(\Delta\phi, \Delta\eta)$ is constructed by pairing the trigger particles in each event with the associated charged particles from 100 different randomly selected events in the same 0.5 cm wide vertex range and from the same track multiplicity class. The same-event and mixed-event pair distributions are first calculated for

each event, and then averaged over the events within the track multiplicity class. The mixed-event distribution is normalized by the sum of background events. The ratio $B(0,0)/B(\Delta\eta,\Delta\phi)$ accounts for pair acceptance effects, with $B(0,0)$ representing the mixed-event associated yield for both particles of the pair going in the same direction and thus having maximum pair acceptance.

Figure 2 (left) shows the two-particle correlation functions for γp-enhanced (upper row) and MB (lower row) events within the multiplicity range $2 \leq N_{\mathrm{trk}} < 35$ as functions of $\Delta\eta$ and $\Delta\phi$. For the γp distribution, the $\Delta\eta$ range is limited to $|\Delta\eta| < 2.5$ by the $\Delta\eta^F$ selection and the acceptance of the tracker. Both distributions show a large jet peak centered at $\Delta\eta = \Delta\phi = 0$, as well as a broader distribution from the recoiling jet centered at $\Delta\eta = 0$ and $\Delta\phi = \pi$. Neither distribution displays a "ridge"-like structure at $|\Delta\phi| \approx 0$ for $|\Delta\eta| > 2$. Figure 2 (right) shows the projections of the two-dimensional correlation functions onto the $\Delta\phi$ axis for $|\Delta\eta| > 2$, away from the jet fragmentation peak. These distributions are fitted over the $\Delta\phi$ range $[0,\pi]$ to a Fourier decomposition series $\propto 1 + \sum_n 2V_{n\Delta}\cos(n\Delta\phi)$, from where the measured $V_{n\Delta}$ are extracted. Only the first three terms are included in the fit, since additional terms have a negligible effect on its quality.

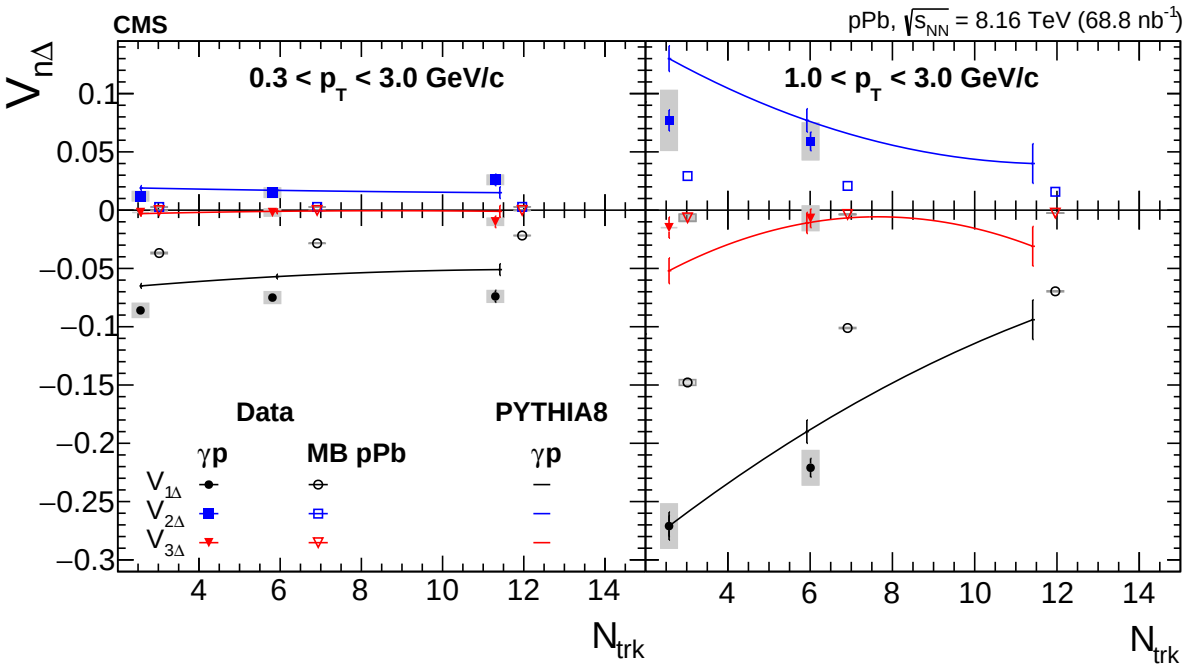

Figure 3: Dependence of $V_{n\Delta}$ on N_{trk} for γp and MB events for two different p_{T} ranges. Systematic uncertainties are shown by the shaded bars in the two panels. The $2 \leq N_{\mathrm{trk}} < 5$, $5 \leq N_{\mathrm{trk}} < 10$, $10 \leq N_{\mathrm{trk}} < 35$ are used for the lower p_{T} range and $2 \leq N_{\mathrm{trk}} < 5$ and $5 \leq N_{\mathrm{trk}} < 35$ for the higher range. The points are placed at the mean value of the corresponding N_{trk} range. Lines indicate the prediction for γp events from PYTHIA8.

5 Systematic uncertainties

The systematic uncertainties of the experimental procedure are evaluated by varying the analysis conditions and extracting new $V_{n\Delta}$ coefficients. The following effects were considered:

1. The systematic uncertainties associated with the choice of the $\Delta\eta^F$ range were estimated

by repeating the analysis with $\Delta\eta^F \in [4.5, 5.0)$, just below the range of the nominal analysis. This alternative selection decreases the purity of the γp-enhanced sample by at most 8% [64]. The size of this uncertainty thus estimated to be 7% for $V_{1\Delta}$ and 27% for $V_{2\Delta}$. For the MB data there is no rapidity gap requirement and so no systematic uncertainty is assigned for this effect.

2. The effect of tracking inefficiency and misreconstructed track rate was studied by varying the track quality requirements. The selection thresholds on the significance of the transverse and longitudinal track impact parameter were varied from 2 to 5 standard deviations. In addition, the relative p_{T} uncertainty is varied from 0.05 to 0.10. This translates into a 3.5% uncertainty in $V_{1\Delta}$ for the $2 \leq N_{\mathrm{trk}} < 5$ category.

3. The sensitivity of the results to the primary vertex position along the beam axis (z_{vtx}) was quantified by comparing events with different z_{vtx} locations from -15 to $+15$ cm. The magnitude of this systematic effect goes up to 150% for $V_{3\Delta}$ with numerical estimations of ± 0.003 for $5 \leq N_{\mathrm{trk}} < 10$ and $10 \leq N_{\mathrm{trk}} < 35$ respectively, in the $0.3 < p_{\mathrm{T}} < 3.0\,\mathrm{GeV}/c$ category, and up to ± 0.013 for $1.0 < p_{\mathrm{T}} < 3.0\,\mathrm{GeV}/c$.

4. The trigger efficiency depends upon N_{trk}. It decreases substantially for $N_{\mathrm{trk}} < 10$, reaching 70% for $N_{\mathrm{trk}} = 2$. To study this effect, a parallel data sample with weighted events as $(1/\varepsilon_{\mathrm{trig}})$ was produced. The full difference of the $V_{n\Delta}$ with and without the correction was taken as the uncertainty. This uncertainty is 2.3% for $V_{1\Delta}$ and 17% for $V_{2\Delta}$ for the sample with $2 \leq N_{\mathrm{trk}} < 5$.

The systematic uncertainties were added in quadrature. For the γp-enhanced sample with $N_{\mathrm{trk}} < 35$ the final uncertainties in $V_{n\Delta}$ are 8.4 and 31% for $n = 1$ and 2, respectively. For the minimum bias sample the uncertainties for $V_{2\Delta}$ are 11% for $2 \leq N_{\mathrm{trk}} < 5$ and smaller than 2.6% for the rest of the N_{trk} range. Since $p_{\mathrm{T}}^{\mathrm{trig}}$ and $p_{\mathrm{T}}^{\mathrm{assoc}}$ have the same range, the fractional uncertainties in v_n are half those of $V_{n\Delta}$.

Table 2: The $V_{n\Delta}$ coefficients for γp-enhanced events, as functions of p_{T} and N_{trk}. Statistical and systematic uncertainties are added in quadrature.

p_{T} range		$2 \leq N_{\mathrm{trk}} < 5$	$5 \leq N_{\mathrm{trk}} < 10$	$10 \leq N_{\mathrm{trk}} < 35$
	$V_{1\Delta}$	-0.086 ± 0.006	-0.075 ± 0.005	-0.074 ± 0.007
$0.3 < p_{\mathrm{T}} < 3.0\,\mathrm{GeV}/c$	$V_{2\Delta}$	0.012 ± 0.004	0.015 ± 0.004	0.026 ± 0.006
	$V_{3\Delta}$	-0.002 ± 0.001	-0.002 ± 0.004	-0.010 ± 0.006
		$2 \leq N_{\mathrm{trk}} < 5$	$5 \leq N_{\mathrm{trk}} < 35$	
	$V_{1\Delta}$	-0.271 ± 0.021	-0.221 ± 0.017	
$1.0 < p_{\mathrm{T}} < 3.0\,\mathrm{GeV}/c$	$V_{2\Delta}$	0.077 ± 0.027	0.059 ± 0.017	
	$V_{3\Delta}$	-0.015 ± 0.009	-0.007 ± 0.013	

6 Results

In order to reduce the contribution to v_n coefficients from back-to-back jet correlations, one can correct v_n by subtracting correlations from very low-multiplicity events (v_n^{sub}), as done in Refs. [4, 53, 68]. Because of the limited N_{trk} range for the γp events (up to $\sim$35), no low multiplicity subtraction is applied to these data. Figure 3 and Table 2 show the measured $V_{n\Delta}$ coefficients as a function of N_{trk} for the two different p_{T} ranges for the γp and MB pPb samples. For the MB sample, the results are consistent with those in [53] before the subtraction procedure. Both

the γp and MB distributions show a negative $V_{1\Delta}$, a positive $V_{2\Delta}$ of smaller magnitude than $V_{1\Delta}$, and a $V_{3\Delta}$ that is consistent with zero. For a given N_{trk} and p_{T} range, both $V_{1\Delta}$ and $V_{2\Delta}$ are larger in the γp samples than in the MB results. For both samples, the magnitude of $V_{1\Delta}$ tends to decrease with N_{trk}, while $V_{2\Delta}$ has at most a weak N_{trk} dependence. Their magnitude are both larger in the higher p_{T} range.

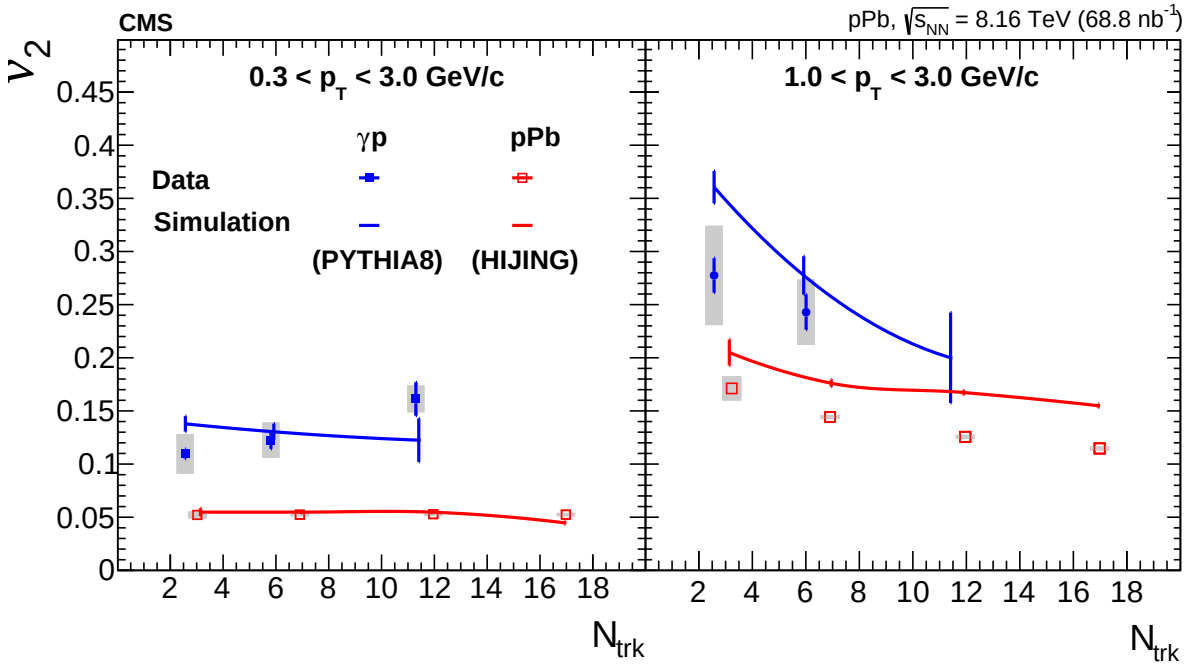

Figure 4: Single-particle azimuthal anisotropy v_2 versus N_{trk} for γp-enhanced and pPb samples in two p_{T} regions. Systematic uncertainties are shown by the shaded bars in the two panels. Predictions from the PYTHIA8 and HIJING generators are shown for the γp and MB pPb samples respectively. For the γp events, same N_{trk} bin arrangement as in Figure 3 is kept while for pPb the bins $[2,5)$, $[5,10)$, $[10,15)$ and $[15,20)$ are used.

Figure 3 also shows predictions from the PYTHIA8 generator for $V_{n\Delta}$ from γp collisions. The predictions of $V_{2\Delta}$ and $V_{3\Delta}$ from PYTHIA8 are reasonably consistent with the γp data and have a similar dependence upon p_{T} and N_{trk}. The $V_{1\Delta}$ prediction is smaller in magnitude than the measured values for the low p_{T}.

Figure 4 shows v_2 as a function of N_{trk} and p_{T} for both γp and MB data sets. For $0.3 < p_{\text{T}} < 3.0\,\text{GeV}/c$, the MB results are consistent with previously published CMS results [53]. Predictions from the PYTHIA8 and HIJING generators are also shown for γp and MB pPb interactions respectively, none of the models include collective effects. For both data and simulations, v_2 varies slowly with track multiplicity for the γp and pPb samples. At a given N_{trk}, v_2 is larger in the higher p_{T} range. This is similar to trends observed in ep collisions [47]. The increase of v_2 with p_{T} is also present in the simulations although both generators slightly overshoot the data at higher p_{T}. For pPb collisions it has been shown that fluctuations in the proton shape can increase v_2 [69]. It is noticeable that at a given p_{T} and N_{trk}, v_2 is higher for γp than for pPb interactions. Tabulated results are provided in the HEPData record for this analysis [70].

7 Summary

For the first time, the study of long-range particle correlations has been extended to photon-proton (γp) interactions. This study used proton-lead (pPb) collisions at $\sqrt{s_{\mathrm{NN}}} = 8.16\,\mathrm{TeV}$ recorded with the CMS detector. The two-particle $V_{n\Delta}$ Fourier coefficients and corresponding single-particle v_2 azimuthal anisotropies are reported as functions of the multiplicity of charged hadrons (N_{trk}) for two transverse momentum (p_{T}) ranges. For the γp sample, the largest observed multiplicity was $N_{\mathrm{trk}} \sim 35$. The mean p_{T} of charged particles is smaller in the γp sample than for pPb collisions within the same multiplicity range. No evidence for a long-range near-side ridge-like structure was found for either the γp or hadronic minimum bias pPb (MB) samples within this multiplicity range. In all N_{trk} and p_{T} ranges, $V_{1\Delta}$ is negative, $V_{2\Delta}$ is positive with a smaller magnitude than $V_{1\Delta}$, and $V_{3\Delta}$ is consistent with zero. The magnitudes of both $V_{1\Delta}$ and $V_{2\Delta}$ increase with p_{T}. This increase has also been seen in electron-proton collisions. At a given p_{T} and track multiplicity, v_2 is larger for γp-enhanced events than for MB pPb interactions. Predictions from the PYTHIA8 and HIJING models describe well the γp and pPb MB data at low p_{T}, but slightly overestimate the data at higher p_{T}. Since these models do not have collective effects, these data suggest the absence of collectivity in the γp system over the multiplicity range explored in this work.

References

[1] CMS Collaboration, "Observation of long-range, near-side angular correlations in proton-proton collisions at the LHC", *JHEP* **09** (2010) 091, doi:10.1007/JHEP09(2010)091, arXiv:1009.4122.

[2] ATLAS Collaboration, "Observation of long-range elliptic azimuthal anisotropies in $\sqrt{s}$ = 13 and 2.76 TeV pp collisions with the ATLAS detector", *Phys. Rev. Lett.* **116** (2016) 172301, doi:10.1103/PhysRevLett.116.172301, arXiv:1509.04776.

[3] CMS Collaboration, "Measurement of long-range near-side two-particle angular correlations in pp collisions at $\sqrt{s} = 13\,\mathrm{TeV}$", *Phys. Rev. Lett.* **116** (2015) 172302, doi:10.1103/PhysRevLett.116.172302, arXiv:1510.03068.

[4] CMS Collaboration, "Evidence for collectivity in pp collisions at the LHC", *Phys. Lett. B* **765** (2017) 193, doi:10.1016/j.physletb.2016.12.009, arXiv:1606.06198.

[5] ATLAS Collaboration, "Measurement of azimuthal anisotropy of muons from charm and bottom hadrons in pp collisions at $\sqrt{s} = 13\,\mathrm{TeV}$ with the ATLAS detector", *Phys. Rev. Lett.* **124** (2020) 082301, doi:10.1103/PhysRevLett.124.082301, arXiv:1909.01650.

[6] CMS Collaboration, "Observation of long-range near-side angular correlations in pPb collisions at the LHC", *Phys. Lett. B* **718** (2013) 795, doi:10.1016/j.physletb.2012.11.025, arXiv:1210.5482.

[7] PHENIX Collaboration, "Measurement of long-range angular correlations and azimuthal anisotropies in high-multiplicity p+Au collisions at $\sqrt{s_{\mathrm{NN}}} = 200\,\mathrm{GeV}$", *Phys. Rev. C* **95** (2017) 034910, doi:10.1103/PhysRevC.95.034910, arXiv:1609.02894.

[8] PHENIX Collaboration, "Creation of quark-gluon plasma droplets with three distinct geometries", *Nature Phys.* **15** (2019) 214, doi:10.1038/s41567-018-0360-0, arXiv:1805.02973.

[9] ATLAS Collaboration, "Observation of associated near-side and away-side long-range correlations in $\sqrt{s_{\rm NN}} = 5.02$ TeV proton-lead collisions with the ATLAS detector", *Phys. Rev. Lett.* **110** (2013) 182302, doi:10.1103/PhysRevLett.110.182302, arXiv:1212.5198.

[10] ATLAS Collaboration, "Measurement with the ATLAS detector of multi-particle azimuthal correlations in p+Pb collisions at $\sqrt{s_{\rm NN}} = 5.02$ TeV", *Phys. Lett. B* **725** (2013) 60, doi:10.1016/j.physletb.2013.06.057, arXiv:1303.2084.

[11] ALICE Collaboration, "Long-range angular correlations on the near and away side in p-Pb collisions at $\sqrt{s_{\rm NN}} = 5.02$ TeV", *Phys. Lett. B* **719** (2013) 29, doi:10.1016/j.physletb.2013.01.012, arXiv:1212.2001.

[12] LHCb Collaboration, "Measurements of long-range near-side angular correlations in $\sqrt{s_{\rm NN}} = 5$ TeV proton-lead collisions in the forward region", *Phys. Lett. B* **762** (2016) 473, doi:10.1016/j.physletb.2016.09.064, arXiv:1512.00439.

[13] ALICE Collaboration, "Long-range angular correlations of π, K and p in pPb collisions at $\sqrt{s_{\rm NN}} = 5.02$ TeV", *Phys. Lett. B* **726** (2013) 164, doi:10.1016/j.physletb.2013.08.024, arXiv:1307.3237.

[14] CMS Collaboration, "Evidence for collective multiparticle correlations in p-Pb collisions", *Phys. Rev. Lett.* **115** (2015) 012301, doi:10.1103/PhysRevLett.115.012301, arXiv:1502.05382.

[15] CMS Collaboration, "Long-range two-particle correlations of strange hadrons with charged particles in pPb and PbPb collisions at LHC energies", *Phys. Lett. B* **742** (2015) 200, doi:10.1016/j.physletb.2015.01.034, arXiv:1409.3392.

[16] ATLAS Collaboration, "Measurement of multi-particle azimuthal correlations in pp, p+Pb and low multiplicity Pb+Pb collisions with the ATLAS detector", *Eur. Phys. J. C.* **77** (2017) 428, doi:10.1140/epjc/s10052-017-4988-1, arXiv:1705.04176.

[17] ATLAS Collaboration, "Measurement of long-range multiparticle azimuthal correlations with the subevent cumulant method in pp and p+Pb collisions with the ATLAS detector at the CERN large hadron collider", *Phys. Rev. C* **97** (2018) 024904, doi:10.1103/PhysRevC.97.024904, arXiv:1708.03559.

[18] J.-Y. Ollitrault, "Anisotropy as a signature of transverse collective flow", *Phys. Rev. D* **46** (1992) 229, doi:10.1103/PhysRevD.46.229.

[19] U. Heinz and R. Snellings, "Collective flow and viscosity in relativistic heavy-ion collisions", *Ann. Rev. Nucl. Part. Sci.* **63** (2013) 123, doi:10.1146/annurev-nucl-102212-170540, arXiv:1301.2826.

[20] C. Gale, S. Jeon, and B. Schenke, "Hydrodynamic modeling of heavy-ion collisions", *Int. J. Mod. Phys. A* **28** (2013) 1340011, doi:10.1142/S0217751X13400113, arXiv:1301.5893.

[21] K. Dusling, W. Li, and B. Schenke, "Novel collective phenomena in high-energy proton–proton and proton–nucleus collisions", *Int. J. Mod. Phys. E* **25** (2016) 1630002, doi:10.1142/S0218301316300022, arXiv:1509.07939.

[22] J. L. Nagle and J. Orjuela Koop, "A quasiparticle transport explanation for collectivity in the smallest of collision systems (p + p and e^+e^-)", *Nucl. Phys. A* **982** (2019) 455, doi:10.1016/j.nuclphysa.2018.09.005, arXiv:1807.04619.

[23] STAR Collaboration, "Elliptic flow in au+au collisions at $\sqrt{s_{\rm NN}} = 130$ GeV", *Phys. Rev. Lett.* **86** (2001) 402, doi:10.1103/PhysRevLett.86.402, arXiv:nucl-ex/0009011.

[24] PHOBOS Collaboration, "System size dependence of cluster properties from two-particle angular correlations in Cu+Cu and Au+Au collisions at $\sqrt{s_{\rm NN}} = 200$ GeV", *Phys. Rev. C* **81** (2010) 024904, doi:10.1103/PhysRevC.81.024904, arXiv:0812.1172.

[25] CMS Collaboration, "Long-range and short-range dihadron angular correlations in central PbPb collisions at a nucleon-nucleon center of mass energy of 2.76 TeV", *JHEP* **10** (2011) 076, doi:10.1007/JHEP07(2011)076, arXiv:1105.2438.

[26] CMS Collaboration, "Centrality dependence of dihadron correlations and azimuthal anisotropy harmonics in PbPb collisions at $\sqrt{s_{\rm NN}} = 2.76$ TeV", *Eur. Phys. J. C* **72** (2012) 10052, doi:10.1140/epjc/s10052-012-2012-3, arXiv:1201.3158.

[27] STAR Collaboration, "Long range rapidity correlations and jet production in high energy nuclear collisions", *Phys. Rev. C* **80** (2009) 064912, doi:10.1103/PhysRevC.80.064912, arXiv:0909.0191.

[28] STAR Collaboration, "Three-particle coincidence of the long range pseudorapidity correlation in high energy nucleus-nucleus collisions", *Phys. Rev. Lett.* **105** (2010) 022301, doi:10.1103/PhysRevLett.105.022301, arXiv:0912.3977.

[29] PHENIX Collaboration, "Formation of dense partonic matter in relativistic nucleus-nucleus collisions at RHIC: Experimental evaluation by the PHENIX collaboration", *Nucl. Phys. A* **757** (2005) 184, doi:10.1016/j.nuclphysa.2005.03.086, arXiv:nucl-ex/0410003.

[30] STAR Collaboration, "Beam-energy dependence of identified two-particle angular correlations in $\sqrt{s_{\rm NN}} = 7.7 - 200$ GeV Au+Au collisions", *Phys. Rev. C* **101** (2020) 014916, doi:10.1103/PhysRevC.101.014916, arXiv:1906.09204.

[31] STAR Collaboration, "Correlation measurements between flow harmonics in Au+Au collisions at RHIC", *Phys. Lett. B* **783** (2018) 459, doi:10.1016/j.physletb.2018.05.076, arXiv:1803.03876.

[32] S. Voloshin and Y. Zhang, "Flow study in relativistic nuclear collisions by fourier expansion of azimuthal particle distributions", *Phys. Rev. C.* **70** (1996) 665, doi:10.1007/s002880050141, arXiv:hep-ph/9407282.

[33] B. H. Alver, C. Gombeaud, M. Luzum, and J.-Y. Ollitrault, "Triangular flow in hydrodynamics and transport theory", *Phys. Rev. C* **82** (2010) 034913, doi:10.1103/PhysRevC.82.034913, arXiv:1007.5469.

[34] C. G. B. Schenke, S. Jeon, "Elliptic and triangular flow in event-by-event D = 3 + 1 viscous hydrodynamics", *Phys. Rev. Lett* **106** (2011) 042301, doi:10.1103/PhysRevLett.106.042301, arXiv:1009.3244.

[35] C. S. Z. Qiu and U. Heinz, "Hydrodynamic elliptic and triangular flow in Pb-Pb collisions at $\sqrt{s_{\rm NN}} = 2.76$ TeV", *Phys. Lett. B* **707** (2012) 151, doi:10.1016/j.physletb.2011.12.041, arXiv:1110.3033.

[36] B. Alver and G. Roland, "Collision geometry fluctuations and triangular flow in heavy-ion collisions", *Phys. Rev. C* **81** (2010) 054905, doi:10.1103/PhysRevC.82.039903, arXiv:1003.0194. [Erratum: Phys. Rev. C 82 (2010) 039903].

[37] CMS Collaboration, "Elliptic flow of charm and strange hadrons in high-multiplicity pPb collisions at $\sqrt{s_{\rm NN}} = 8.16$ TeV", *Phys. Rev. Lett.* **121** (2018) 082301, doi:10.1103/PhysRevLett.121.082301, arXiv:1804.09767.

[38] CMS Collaboration, "Centrality and pseudorapidity dependence of the transverse energy density in pPb collisions at $\sqrt{s_{\rm NN}} = 5.02$ TeV", *Phys. Rev. C* **100** (2019) 024902, doi:10.1103/PhysRevC.100.024902, arXiv:1810.05745.

[39] ALICE Collaboration, "Multi-strange baryon production in pPb collisions at $\sqrt{s_{\rm NN}} = 5.02$ TeV", *Phys. Lett. B* **758** (2016) 389, doi:10.1016/j.physletb.2016.05.027, arXiv:1512.07227.

[40] PHENIX Collaboration, "Elliptic flow of identified hadrons in Au+Au collisions at $\sqrt{s_{\rm NN}} = 200$ GeV", *Phys. Rev. Lett.* **91** (2003) 182301, doi:10.1103/PhysRevLett.91.182301, arXiv:nucl-ex/0305013.

[41] STAR Collaboration, "Distributions of charged hadrons associated with high transverse momentum particles in pp and Au+Au collisions at $\sqrt{s_{\rm NN}} = 200$ GeV", *Phys. Rev. Lett.* **95** (2005) 152301, doi:10.1103/PhysRevLett.95.152301, arXiv:nucl-ex/0501016.

[42] R. D. Weller and P. Romatschke, "One fluid to rule them all: viscous hydrodynamic description of event-by-event central p+p, p+Pb and Pb+Pb collisions at $\sqrt{s} = 5.02$ TeV", *Phys. Lett. B* **774** (2017) 351, doi:10.1016/j.physletb.2017.09.077, arXiv:1701.07145.

[43] P. Bozek, "Collective flow in p-Pb and d-Pb collisions at TeV energies", *Phys. Rev. C* **85** (2012) 014911, doi:10.1103/PhysRevC.85.014911, arXiv:1112.0915.

[44] P. Bozek and W. Broniowski, "Correlations from hydrodynamic flow in p-Pb collisions", *Phys. Lett. B* **718** (2013) 1557, doi:10.1016/j.physletb.2012.12.051, arXiv:1211.0845.

[45] P. Bozek and W. Broniowski, "Collective dynamics in high-energy proton-nucleus collisions", *Phys. Rev. C* **88** (2013), no. 1, 014903, doi:10.1103/PhysRevC.88.014903, arXiv:1304.3044.

[46] A. Badea et al., "Measurements of two-particle correlations in e^+e^- collisions at 91 GeV with ALEPH archived data", *Phys. Rev. Lett.* **123** (2019) 212002, doi:10.1103/PhysRevLett.123.212002, arXiv:1906.00489.

[47] ZEUS Collaboration, "Two-particle azimuthal correlations as a probe of collective behaviour in deep inelastic ep scattering at HERA", *JHEP* **04** (2020) 070, doi:10.1007/JHEP04(2020)070, arXiv:1912.07431.

[48] ATLAS Collaboration, "Two-particle azimuthal correlations in photonuclear ultraperipheral Pb+Pb collisions at 5.02 TeV with ATLAS", *Phys. Rev. C* **104** (2021) 014903, doi:10.1103/PhysRevC.104.014903, arXiv:2101.10771.

[49] A. J. Baltz, "The physics of ultraperipheral collisions at the LHC", *Phys. Rept.* **458** (2008) 1, doi:10.1016/j.physrep.2007.12.001, arXiv:0706.3356.

[50] C. F. von Weizsäcker, "Radiation emitted in collisions of very fast electrons", *Z. Phys.* **88** (1934) 612, doi:10.1007/BF01333110.

[51] E. J. Williams, "Nature of the high-energy particles of penetrating radiation and status of ionization and radiation formulae", *Phys. Rev.* **45** (1934) 729, doi:10.1103/PhysRev.45.729.

[52] E. Fermi, "On the theory of collisions between atoms and electrically charged particles", *Nuovo Cim.* **2** (1925) 143, doi:10.1007/BF02961914, arXiv:hep-th/0205086.

[53] CMS Collaboration, "Observation of correlated azimuthal anisotropy fourier harmonics in pp and p+Pb collisions at the LHC", *Phys. Rev. Lett.* **120** (2018) 092301, doi:10.1103/PhysRevLett.120.092301, arXiv:1709.09189.

[54] I. Helenius and C. O. Rasmussen, "Hard diffraction in photoproduction with PYTHIA 8", *Eur. Phys. J. C* **79** (2019), no. 5, 413, doi:10.1140/epjc/s10052-019-6914-1, arXiv:1901.05261.

[55] DELPHES 3 Collaboration, "DELPHES 3, a modular framework for fast simulation of a generic collider experiment", *JHEP* **02** (2014) 057, doi:10.1007/JHEP02(2014)057, arXiv:1307.6346.

[56] X.-N. Wang and M. Gyulassy, "HIJING: A monte carlo model for multiple jet production in pp, pA and AA collisions", *Phys. Rev. D* **44** (1991) 3501, doi:10.1103/PhysRevD.44.3501.

[57] GEANT4 Collaboration, "GEANT4—a simulation toolkit", *Nucl. Instrum. Meth. A* **506** (2003) 250, doi:10.1016/S0168-9002(03)01368-8.

[58] O. Surányi, "Performance of the CMS zero degree calorimeters in the 2016 pPb run", *J. Phys. Conf. Ser.* **1162** (2019) 012005, doi:10.1088/1742-6596/1162/1/012005.

[59] CMS Collaboration, "Particle-flow reconstruction and global event description with the CMS detector", *JINST* **12** (2017) P10003, doi:10.1088/1748-0221/12/10/P10003, arXiv:1706.04965.

[60] CMS Collaboration, "The CMS experiment at the CERN LHC", *JINST* **3** (2008) S08004, doi:10.1088/1748-0221/3/08/S08004.

[61] CMS Collaboration, "Description and performance of track and primary-vertex reconstruction with the CMS tracker", *JINST* **9** (2014) P10009, doi:10.1088/1748-0221/9/10/P10009, arXiv:1405.6569.

[62] CMS Collaboration, "The CMS trigger system", *JINST* **12** (2017) P01020, doi:10.1088/1748-0221/12/01/P01020, arXiv:1609.02366.

[63] CMS Collaboration, "Pseudorapidity distributions of charged hadrons in proton-lead collisions at $\sqrt{s_{\mathrm{NN}}} = 5.02$ and 8.16 TeV", *JHEP* **01** (2018) 045, doi:10.1007/JHEP01(2018)045, arXiv:1710.09355.

[64] CMS Collaboration, "First measurement of the forward rapidity gap distribution in pPb collisions at $\sqrt{s_{\mathrm{NN}}} = 8.16\,\mathrm{TeV}$", Technical Report CMS-PAS-HIN-18-019, 2020.

[65] ATLAS Collaboration, "Rapidity gap cross sections measured with the ATLAS detector in pp collisions at $\sqrt{s} = 7\,\mathrm{TeV}$", *Eur. Phys. J. C* **72** (2012) 1926, doi:10.1140/epjc/s10052-012-1926-0, arXiv:1201.2808.

[66] CMS Collaboration, "Measurement of diffraction dissociation cross sections in pp collisions at $\sqrt{s} = 7\,\mathrm{TeV}$", *Phys. Rev. D* **92** (2015) 012003, doi:10.1103/PhysRevD.92.012003, arXiv:1503.08689.

[67] J. D. Bjorken, "Rapidity gaps and jets as a new physics signature in very high-energy hadron hadron collisions", *Phys. Rev. D* **47** (1993) 101, doi:10.1103/PhysRevD.47.101.

[68] CMS Collaboration, "Multiplicity and transverse momentum dependence of two- and four-particle correlations in pPb and PbPb collisions", *Phys. Lett. B* **724** (2013) 213, doi:10.1016/j.physletb.2013.06.028, arXiv:1305.0609.

[69] H. Mäntysaari, B. Schenke, C. Shen, and P. Tribedy, "Imprints of fluctuating proton shapes on flow in proton-lead collisions at the LHC", *Phys. Lett. B* **772** (2017) 681, doi:10.1016/j.physletb.2017.07.038, arXiv:1705.03177.

[70] "HEPData record for this analysis", 2022. doi:10.17182/hepdata.89877.